THE JOURNAL OF BIOLOGICAL CHEMISTRY VOL. 290, NO. 49, pp. 29531–29541, December 4, 2015

Structural Basis of Neuronal Nitric-oxide Synthase Interaction with Dystrophin Repeats 16 and 17*

Received for publication, July 24, 2015, and in revised form, September 11, 2015 Published, JBC Papers in Press, September 16, 2015, DOI 10.1074/jbc.M115.680660

Anne-Elisabeth Molza[‡§1,2], **Khushdeep Mangat**[¶1,3], **Elisabeth Le Rumeur**[‡§], **Jean-François Hubert**[‡§], **Nick Menhart**[¶], **and Olivier Delalande**[‡§4]

From the [‡]*Université de Rennes1, Campus Santé, 35043 Rennes, France, the* [§]*Institut de Génétique et Développement de Rennes, IGDR, UMR CNRS 6290, Rennes, France, and the* [¶]*Illinois Institute of Technology, Chicago, Illinois 60616*

Background: Nitric-oxide synthase (NOS) function in skeletal muscles is due to its interaction with dystrophin.
Results: We developed a structural model of NOS and dystrophin interaction by biochemical and *in silico* approaches.
Conclusion: Our study provides insights about the proper localization of NOS in skeletal muscle.
Significance: The molecular details of the interaction are crucial for gene therapy optimization to treat Duchenne patients.

Duchenne muscular dystrophy is a lethal genetic defect that is associated with the absence of dystrophin protein. Lack of dystrophin protein completely abolishes muscular nitric-oxide synthase (NOS) function as a regulator of blood flow during muscle contraction. In normal muscles, nNOS function is ensured by its localization at the sarcolemma through an interaction of its PDZ domain with dystrophin spectrin-like repeats R16 and R17. Early studies suggested that repeat R17 is the primary site of interaction but ignored the involved nNOS residues, and the R17 binding site has not been described at an atomic level. In this study, we characterized the specific amino acids involved in the binding site of nNOS-PDZ with dystrophin R16–17 using combined experimental biochemical and structural *in silico* approaches. First, 32 alanine-scanning mutagenesis variants of dystrophin R16–17 indicated the regions where mutagenesis modified the affinity of the dystrophin interaction with the nNOS-PDZ. Second, using small angle x-ray scattering-based models of dystrophin R16–17 and molecular docking methods, we generated atomic models of the dystrophin R16–17·nNOS-PDZ complex that correlated well with the alanine scanning identified regions of dystrophin. The structural regions constituting the dystrophin interaction surface involve the A/B loop and the N-terminal end of helix B of repeat R16 and the N-terminal end of helix A′ and a small fraction of helix B′ and a large part of the helix C′ of repeat R17. The interaction surface of nNOS-PDZ involves its main β-sheet and its specific C-terminal β-finger.

Mutations of the dystrophin *DMD*[5] gene lead to the two devastating Duchenne muscular dystrophy (DMD) and Becker muscular dystrophy (BMD) due to a complete loss of the protein or to the production of modified dystrophin, respectively (1–3). These diseases are characterized by a progressive muscle weakness that is fatal for most DMD patients before they reach the age of 30. Effective treatment for this disease does not exist, although several human clinical trials are in progress (4, 5). Dystrophin is a large filamentous scaffolding protein situated at the costameres in striated muscle fibers. It is composed of four major domains (6). The N-terminal end is an actin-binding domain acting with two calponin homology domains; the central domain is made up of 24 spectrin-like repeats interspaced by four hinges and interacts with a large number of filamentous proteins, such as actin, microtubules, and intermediate filaments, with the cytosolic proteins PAR1 and neuronal NOS (nNOS) and with membrane phospholipids; the Cys-rich domain interacts with the membrane protein β-dystroglycan and the C-terminal domain through syntrophin and dystrobrevin. A major portion of these protein partners are thus localized at the sarcolemma through their binding to dystrophin, by which they contribute to the constitution of a direct link between the cytoskeleton and extracellular matrix.

In DMD and BMD, the primary muscle defects are disruptions of this dystrophin scaffolding network, which lead to loss of fibers and muscle weakness. Among these modifications, nNOS recruitment at the sarcolemma is impaired due to the dystrophin deficit or mutation. Indeed, nNOS delivers the diffusible signaling molecule nitric oxide (NO) into circulation, inducing a functional local vasodilation that is essential for normal oxygenation of the exercising muscles (7–9). A deficit in its sarcolemma localization impairs functional muscle vasodilatation in DMD, which leads to ischemia and muscle damage (8). This effect participates in the muscle weakness of DMD (10). In BMD patients, maintenance of nNOS at the sarcolemma through interaction with modified dystrophin is accompanied by a less severe phenotype compared with that of patients in whom nNOS sarcolemma localization is lost (11).

* This work was supported in part by the Association Française Contre les Myopathies, AFM-Téléthon, Rennes Métropole, the Grand Equipement National de Calcul Intensif-GENCI program (projet DARI DYSIM), and Muscular Dystrophy Association, USA Grant 217640.
[1] Both authors contributed equally to this work.
[2] Supported by AFM-Téléthon for a PhD thesis.
[3] Supported by Rennes Metropole for a stay at the IGDR in France.
[4] To whom correspondence should be addressed: Faculté des Sciences Pharmaceutiques et Biologiques, Université de Rennes 1, IGDR, UMR CNRS 6290, Équipe SIM, Plateforme PRISM, 2 Av. Pr. Leon Bernard CS 34317, 35043 RENNES Cedex France. Tel.: 332-23-23-30-07; Fax: 332-23-23-46-06; E-mail: olivier.delalande@univ-rennes1.fr.

[5] The abbreviations used are: DMD, Duchenne muscular dystrophy; BMD, Becker muscular dystrophy; nNOS, neuronal nitric-oxide synthase; SAXS, small angle x-ray scattering.

NOS enzymes comprise a large family of homodimeric proteins that are involved in different signaling pathways (12–14). In muscle cells, the nNOSμ isoform is especially involved in the interaction with dystrophin. Structurally, all NOS isoforms comprise a catalytic domain and a calmodulin-binding domain. nNOSμ also includes a PDZ domain with a specific β-finger that is not present in classical PDZ domains (15, 16). This enzyme was first shown to interact with syntrophin through a non-canonical interaction of their respective PDZ domains, notably involving the nNOS-PDZ β-finger (15). Recently, repeats R16 and R17 of the central domain of dystrophin, two spectrin-like repeats theoretically organized in a coiled-coil fold of three α-helices A, B, and C for R16 and A′, B′, and C′ for R17, were shown to constitute an nNOS interaction site that is distant from the dystrophin C-terminal region that associates with syntrophin (17–19). This explains why the presence of syntrophin at the sarcolemma through its association with dystrophin did not always maintain nNOS localization as in BMD cases (11). However, whereas several rat experimental structures of the nNOS-PDZ domain were obtained (15, 20), no experimental structure of the dystrophin R16–17 fragment is yet available.

Through investigations using *in vivo* and cellular systems, the nNOS-PDZ dystrophin-binding site was suggested to be located in a 10-residue fragment in dystrophin R17. This primary site also needed to be framed by the not-yet-precisely defined parts of repeats 16 and 17. A yeast two-hybrid assay and an *in vivo* assay led to the same conclusion of the involvement of this 10-residue long site in repeat 17, but contrasting conclusions were drawn about the other parts of the two repeats involved in the binding (18). However, these *in vivo* experiments did not take into account the three-dimensional aspects of the binding, which are needed to improve our understanding of the normal mechanisms of the interaction and how the BMD mutations could interfere with these interaction mechanisms. Therefore, a detailed three-dimensional molecular description of the binding site is lacking. In addition, the dystrophin binding site on nNOS was not studied.

In the present study, we proposed the description of the structural molecular details of this interaction on both proteins at an atomic level using an *in vitro* alanine-scanning mutagenesis experiment combined with a structural *in silico* analysis. The two approaches converged to show that the binding site of dystrophin R16–17 repeats to nNOS-PDZ involves the loop between helix A and B of repeat 16 and a large part of repeat 17. By contrast, the dystrophin binding site of nNOS involves the β-finger and the main β-sheet of the protein. Analysis of the sequence similarities of the site to its modifications in several BMD deletions provides clues about the nNOS sarcolemma localization in these pathologies.

Experimental Procedures

Biochemical Analysis of the Dystrophin R16–17 and nNOS-PDZ Binding

Protein Expression and Purification of Dystrophin R16–17 and the Variants—An alanine scan was conducted using our previously described R16–17 construct by replacing all the charged residues in exons 42 to 45 in 32 groups of 1 to 5 into an alanine. Cloning of the wild-type R16–17 was performed as previously described in detail (21). One additional variant was made from a previously chimeric construct shown to perturb nNOS binding within R16–17 (18). This mutation changes 7 dystrophin residues to the homologous utrophin sequence (Fig. 1*A*). The mutant genes were constructed by Gibson assembly (22) and sequenced to ensure correct constructions. The expression and production of these target proteins followed a previously described protocol (21).

Protein Expression and Purification of PDZ Domains of nNOS and Syntrophin—The PDZ domains of syntrophin (SNTA-PDZ) and nNOS (nNOS-PDZ) were expressed using the same GST affinity tag system that was used for the dystrophin variants. These constructs were based on the known crystal structure of nNOS-PDZ·SNTA-PDZ complex (15), and include the β-finger region of nNOS-PDZ (Fig. 2*A*). Both constructs were cloned in the pGEX expression plasmid. The ion exchange step is a unique step due to the specific charge properties of each protein. For nNOS-PDZ, we did not release nNOS-PDZ from GST by proteolysis so that during biotinylation, the much larger GST (25 kDa) would provide most of the lysine residues to which biotin could be coupled. We biotinylated at a low (0.8 to 2) ratio to ensure that most molecules had biotins attached to the GST motif and not to the PDZ motif to minimize perturbations of this bait region. To complete the purification of GST-nNOS-PDZ and SNTA-PDZ, ion exchange chromatography was conducted using HiTrapQ resin (GE Life Sciences) using a buffer of Tris, pH 8.5.

Biophysical Characterization of the Wild-type and Mutated Variants of Dystrophin R16–17 and nNOS-PDZ—To examine the secondary structure, we placed proteins at A_{280} ~0.5–1.0 in PBS (5 mM phosphate, pH 7.4, 150 mM NaCl) in a 1-mm cell and circular dichroism (CD) spectra from 300 to 190 nm. Helicity was assessed from the intensity at 222 nm, the α-helix signature region (21). To assess thermodynamic stability, we subjected the proteins to a thermal scan from 10 to 98 °C at 1 °C/min, whereas the CD signal θ_{222} was monitored. The resulting data were fit to a two-state thermodynamic model provided as previously described, yielding the melting temperature, T_m (21). For the nNOS-PDZ motif, thermal unfolding was instead monitored at 208 nm, which confirmed its β-strand-dominated secondary structure.

Binding Experiments

Biotinylation—For the optical surface, we used the commonly employed biotin/streptavidin interaction because of its gentle yet irreversible non-covalent binding. A commercially available streptavidin-coated tip (Fortebio) was biotinylated with the bait protein GST-nNOS-PDZ. To this end, the bait protein GST-nNOS-PDZ or the control GST protein at ~1 mg/ml in PBS was incubated with a 5-fold molar excess of Chromalink (Solulink Inc.) for 60 min at 25 °C in the dark. This biotinylation reagent couples to lysine residues through a *N*-hydroxy-succinamide reactive ester and has a spacer consisting of a 15-atom hydrophilic PEG region and a bisaryl hydrazone chromophore that absorbs at 354 nm to facilitate the quantification of labeling. Excess Chromalink was quenched by the

addition of 1 volume of 1 M Tris, pH 8.5, removed by desalting over a 0.5 × 10-cm column of Sephadex G50 in PBS, and then dialyzed against PBS overnight. The biotinylation ratios were controlled by altering the incubation time and NCB ratio in preliminary experiments and were determined by the known ϕ_{354} = 29,000 and ϕ_{280} = 7825 of the bis-arylhydrazone chromophore and the ϕ_{280} of the target protein as determined from its amino acid sequence. The final biotinylation ratios were 1:2. The streptavidin optical surface was coated by dipping in biotinylated protein at a concentration of 9 μM in PBS for 120 s. The tip was then washed in PBS binding buffer, PBSBB (1× PBS, 0.1 mg/ml of BSA, 0.002% Tween 20) for 180 s and stored at 4 °C in PBSBB until use.

Binding Affinity Determination—Binding experiments were performed using the Biolayer Interferometry system (BLItz; Fortebio). In this system, bait proteins are immobilized on the surface of a glass optical guide, and the thickness of this protein boundary layer was probed by interferometry. In a binding experiment, the probe surface was dipped into a solution of the target protein at various concentrations, and association was monitored by changes in the intensity of the interference signal. Once binding is complete, the probe surface can then be transferred back to a target protein-free dissociation buffer solution to both regenerate the surface and monitor dissociation.

All the binding experiments were conducted in PBSBB. A serial 1:2 dilution of target protein into PBSBB was prepared. For dystrophin R16–17, which displayed K_D ~50 μM toward nNOS-PDZ, an upper concentration of 400 μM was typically used. Aliquots of the protein were serially diluted 1:2 into PBSBB to produce a series that typically included 8 concentrations. For dystrophin R16–17 and its variants a series between 400 and 3.2 μM was performed, whereas for SNTA-PDZ the series was typically between 50 and 0.78 μM.

Binding was assessed by acquiring the baseline interference intensity signal with the optical surface immersed in PBSBB for 30 s; the surface was then transferred to the target protein aliquot at some given concentration for 30 s and then transferred to a 550-μl aliquot of PBSBB for 60 s to dissociate. During this process, the interference intensity signal was acquired, which can in principle provide the k_{on} and k_{off} rates. For the SNTA-PDZ/nNOS-PDZ interaction, this provision was the case. Unfortunately, for the dystrophin R16–17/PDZ-nNOS interaction, the binding kinetics were strongly non-exponential, and a multiphasic behavior was observed. This precluded reliable assessment of the on and off rates. Therefore, only the equilibrium extent of the binding was used to assess the binding strength. Thus, the final extent of the binding signal was fit to the Langmuir equation, $d = S/(K_d + S)$ to yield a K_D. To ensure reproducibility, the experiments were conducted at least 3 times on different days with different coated surfaces, and independent K_D determinations were averaged. In all cases, the control SNTA-PDZ/nNOS-PDZ interaction runs were obtained immediately before and after each dystrophin R16–17 variant test to ensure that the different surfaces behaved identically during these different runs. Differences in binding affinities for the alanine-scanned variants were determined by a two-tailed Student's t test between the K_D measurements of each variant and a similar group of measurements on wild-type dystrophin R16–17. Significance was accepted at the $p < 0.05$ level.

In Silico Construction of a Dystrophin R16–17·nNOS-PDZ Complex

Human nNOS-PDZ Domain and Dystrophin R16–17 Three-dimensional Structural Models—A model of the human nNOS-PDZ (UniProt P29476) was computed by homology modeling through the I-TASSER web server (23) with rat structure as the major template (Protein Data Bank code 1QAU).

The two dystrophin R16–17 models used in this study were previously obtained using small-angle x-ray scattering and molecular dynamics (24). SAXS measurements were conducted at the French synchrotron SOLEIL (St. Aubin, France) on the SWING beamline. A stock solution of the sample was prepared at a final concentration of 8 mg/ml and stored at 4 °C before being injected into the online HPLC system (Agilent) installed upstream of the SAXS capillary for experiments at SWING (SEC-SAXS)(25). Data analysis was completed with the ATSAS suite (26, 27), using the GASBOR program to generate *ab initio* models. The molecular models were built from the two *ab initio* low-resolution shapes, which were best correlated to the scattering data (both $\chi 2$ = 2.53). They displayed moderate differences in their molecular organization (comparative NSD of 1.02 Å). Respective final models well fit to their initial SAXS low-resolution shapes (volume cross-correlation of 88% for model 1 and 92% for model 2). Dystrophin R16–17 structural models are composed of two triple helical coiled-coils bridged by a kinked linker region (49° and 50° for models 1 and 2, respectively). The two models were obtained with a high quality score, and we used these to compute theoretical complexes with nNOS-PDZ.

R16–17·nNOS-PDZ Complex by Low Resolution Rigid Docking—Rigid docking was performed using ATTRACT software (28) with the previously obtained models. Dystrophin R16–17, given its large size, was considered the receptor and nNOS-PDZ the ligand. The two dystrophin R16–17 models were obtained through an SAXS-driven flexible fitting procedure and allowed to modulate the receptor shape during the first step consisting of static low resolution docking. The models were reduced according to the Zacharias force field, with one amino acid being described by one to three coarse grains (28). The nNOS-PDZ starting position was defined using a density grid of 10 Å around dystrophin R16–17. Thus, almost 100,000 complexes were calculated from 381 and 402 starting positions of the ligand distributed around R16–17 models 1 and 2 as receptors, respectively. For both models, 258 rotations were applied to each starting position to modulate the relative orientation of both protein partners. The rigid docking results were analyzed through an energy evaluation of the theoretical complexes and by clustering the complexes using a root mean square deviation of 10 Å according to the ligand final position. The 20 best theoretical complexes, *i.e.* the most populated clusters with the lowest ATTRACT energy complexes, were selected to compute the contact frequencies between the two proteins (cut-off distance of 5 Å).

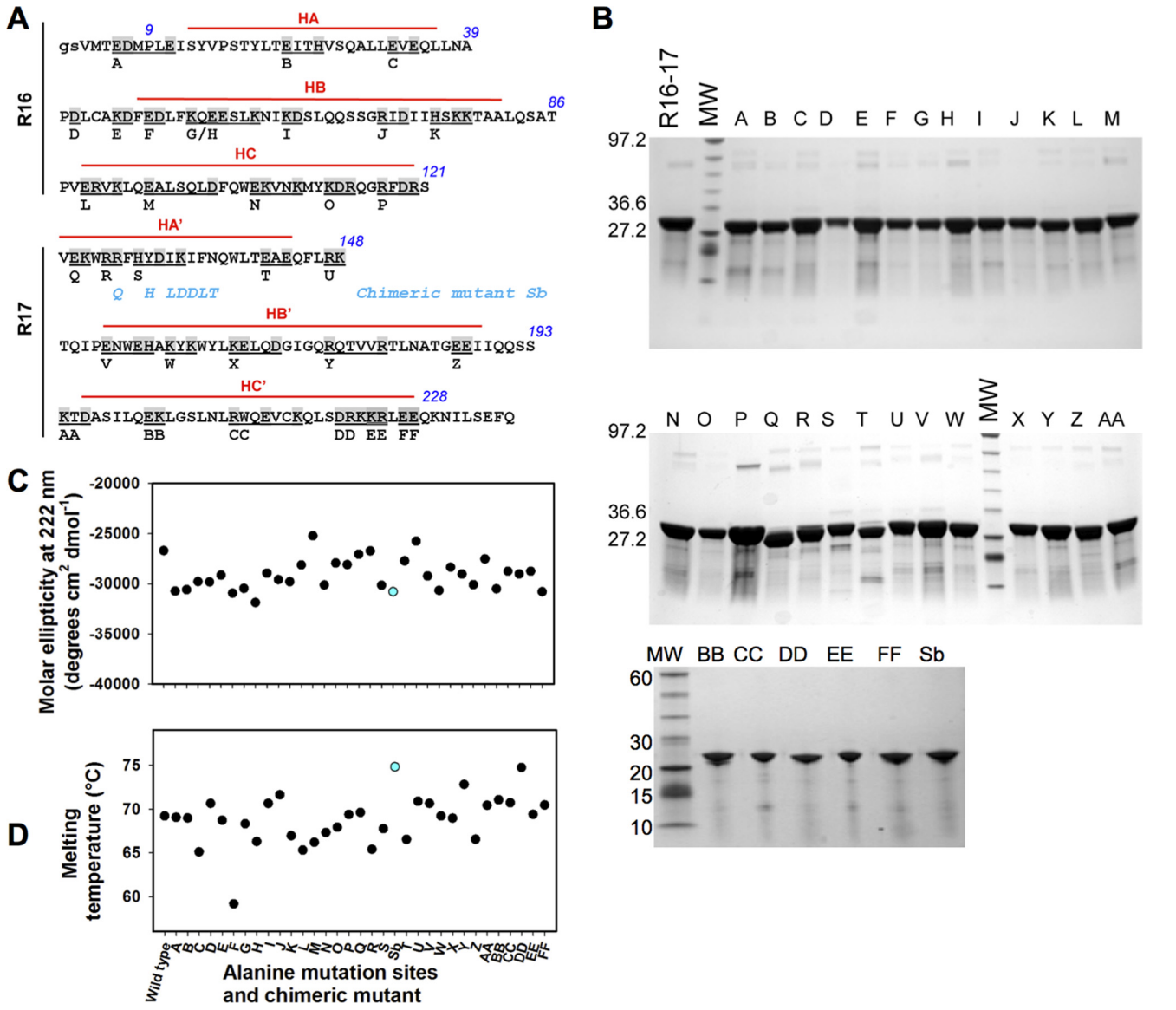

FIGURE 1. **Biochemical characterization of the dystrophin R16–17 fragment and mutants.** *A,* for alanine-scanning mutagenesis, all charged residues of dystrophin R16–17 were changed to alanine in groups of 1 to 5 amino acids (common value of 2–3 amino acids). This grouping encompassed 74 residues (shown in *gray*), resulting in 32 variants, A through FF. The *capital letters* are the R16 and R17 sequence according to Koenig and Kunkel (38); the *gs* italicized letters are residues present due to cloning constraints. The three helices of each repeat are indicated in *red lines* and noted as HA, HB, and HC for repeat 16 and HA′, HB′, and HC′ for repeat 17. The residues *not marked by red lines* are those involved in the loops between successive helices. There is no interruption of the HC and HA′ of repeats 16 and 17, respectively, with these two helices forming a common helix with the residues in the junction involved in the so-called linker. The chimeric mutant Sb not corresponding to alanine-scanning mutagenesis is shown: the *blue* residues are those substituted from the utrophine sequence. *B,* the native fragment of dystrophin R16–17, the 32 alanine mutants, and the chimeric Sb mutant were produced and purified. The fragments appeared at the expected molecular masses of ~22,700 Da and at a high degree of purity. *MW*, molecular weight standards. *C,* molar ellipticity values at 222 nm as measured from CD spectra for the wild-type dystrophin R16–17 and all the mutants. The chimeric mutant value appears in *blue*. *D,* melting temperatures of wild-type dystrophin R16–17 and all the mutants as obtained by heating from 15 to 85 °C and followed by CD at 222 nm. The chimeric mutant value appears in *blue*.

R16–17·nNOS-PDZ Complex by Interactive Flexible Docking—The best theoretical complexes obtained by rigid docking were used as either a starting position or a target position for flexible interactive docking simulation using the BioSpring program (29). To take into account the different secondary structural elements of nNOS-PDZ while allowing a sufficient degree of freedom for flexible docking, we chose a multiple distance cut-off to define backbone particles as previously described (24). Both proteins were converted to an augmented Elastic Network Model, which links by a spring two particles when they are closer than the cut-off distances. An electrostatic potential grid of R16–17 was calculated using the APBS program (30), the Amber force field and 50 mM sodium and chloride ions, to guide nNOS-PDZ using a Phantom Omni Sensable haptic device (29).

Optimization and Quality Control of the R16–17·nNOS-PDZ Complex Model—For each complex, 10 independent simulated annealing procedures were performed in YASARA using the YAMBER3 force field (31). During simulated annealing, the peptide backbone was first fixed for the amino acids involved in secondary structure elements according to DSSP measurements (32). Under the following energy minimization cycles, the α carbons of the same residues were fixed and then released. Quality control of atomic models (20 complex structures) was

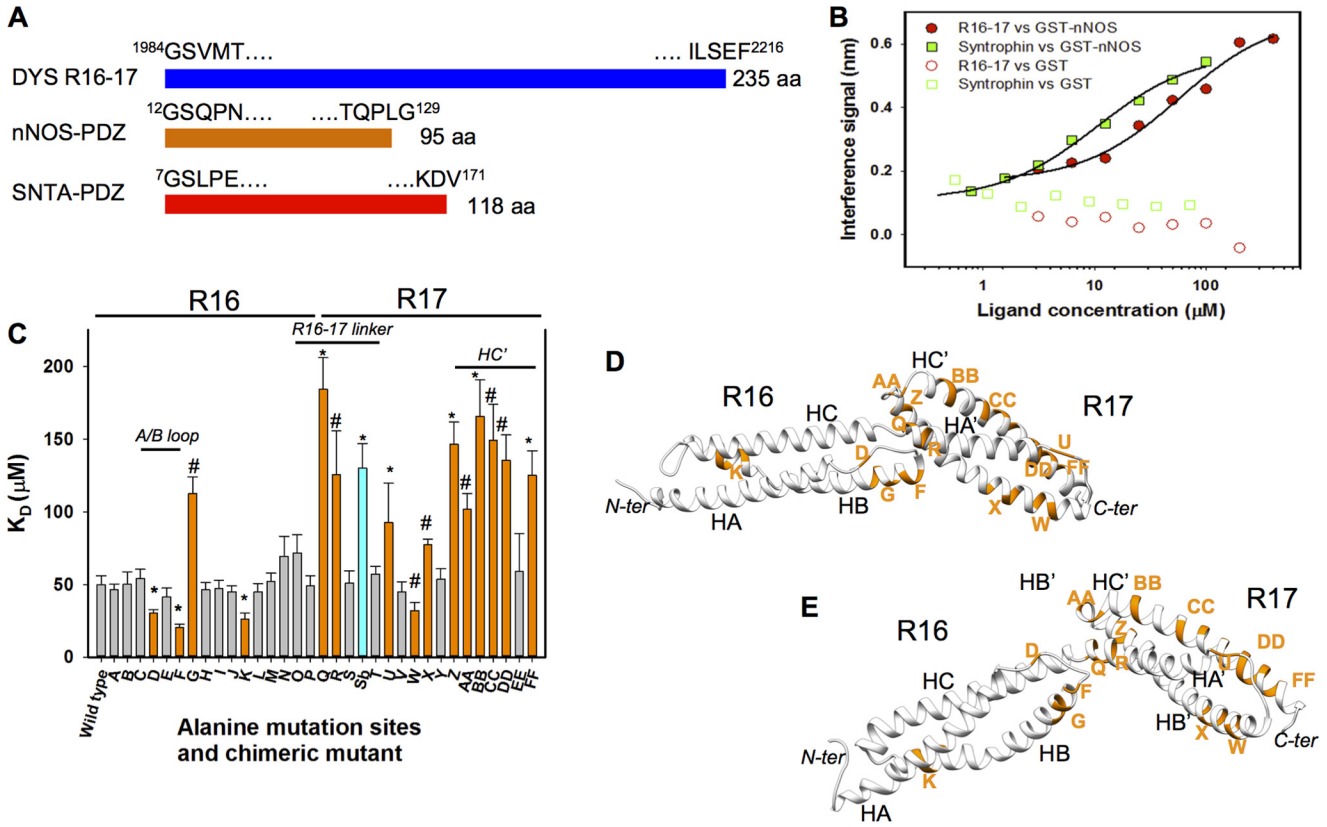

FIGURE 2. **Consequences of the alanine mutation scan of dystrophin R16–17 on the dissociation constant with nNOS-PDZ.** *A*, schematic representation of the three constructs used for the affinity measurements: dystrophin repeats R16 and R17 (*DYS R16–17*), nNOS-PDZ domain, and the syntrophin PDZ domain (*SNTA-PDZ*). The residues at the N- and C-terminal ends are shown together with the residue numbering in the whole protein. The number of amino acids of each fragment is indicated at the extreme *right*. *B*, binding curves for nNOS-PDZ-dystrophin R16–17 and nNOS-PDZ-SNTA-PDZ showed a K_D of 50 ± 6 and 7.2 ± 1.2 μM, respectively. Controls with GST are also shown. *C*, dissociation constants (K_D values) of the binding of nNOS-PDZ to dystrophin R16–17 and all the mutants. Values for the wild-type are the mean ± S.D. of 12 similar assays. The values are the mean ± S.D. for 3 to 6 similar assays of the mutants. The values that are significantly different from those for the wild-type are shown in *orange*. *, for $p < 0.005$; #, for $p < 0.05$. The value of the chimeric mutant is shown in *blue*. *D* and *E*, the mutated sites with significantly different values are shown in *orange* on the two three-dimensional dystrophin R16–17 models 1 and 2 represented as a *gray schematic*. The three helices of each repeat are noted as in Fig. 1*A*. The models are shown with the N-terminal end (*N-ter*) on the *left* and the C-terminal end (*C-ter*) on the *right*.

performed using Procheck and Errat included in the Structure Analysis And Validation Server (SAVES version 4), DSSP for helix percentage calculations and Naccess for surface-accessible solvent measurements as needed to evaluate the contact surface.

Molecular Surface Potential Analysis and Visualization—To compare the hydrophobic/hydrophilic properties of the models, the molecular hydrophobicity potential was calculated using the PLATINUM web server (33). A molecular hydrophobicity potential scale shift of 0.03 was applied to obtain a realistic distribution of the hydrophobic properties of the molecules. The electrostatic potential surfaces were computed using the Protein Data Bank code 2PQR (34) and the Adaptive Poisson-Boltzmann Solver (APBS) (30) programs. All the molecular structures and potentials were visualized and rendered with the Chimera (35), VMD (36), and PyMOL programs.

In Silico Alanine Mutation—*In silico* alanine-scanning mutagenesis was performed by using the FoldX plugin (37) for YASARA (FoldX version 3.0). The binding free energy changes ($\Delta\Delta G$) were computed in kcal/mol. The values are given as the average of three runs for $T = 298$ K, pH 7, and an ionic strength of 0.05 M.

Results

In Vitro Binding of Dystrophin R16–17 and nNOS-PDZ

Stability Analysis of Dystrophin R16–17 Variants After Alanine Mutagenesis—To experimentally map the binding site of dystrophin R16–17 to nNOS-PDZ at a residue level, we performed an alanine site-directed mutagenesis scanning along the dystrophin R16–17 sequence. One to five charged residues that were close in sequence were mutated at once in alanine, and we thus obtained 32 constructs named A to FF (Fig. 1*A*). All appeared as single bands as shown by SDS-polyacrylamide gels (Fig. 1*B*). Because the mutations will potentially affect the structure and/or stability of the protein, we screened all the mutated proteins for both secondary structure and thermodynamic stability by circular dichroism (CD) spectroscopy as previously done (21). All the mutated proteins exhibited CD spectra typical of α helical proteins. Their molar ellipticity at 222 nm was measured between −25,000 and −32,000 degrees cm^2 $dmol^{-1}$ (Fig. 1*C*), which corresponded to folding in α helices. In several cases, a slight increase in helicity was observed, which is not surprising because alanine is a strong helix-stabilizing residue. To determine whether the mutated proteins remained stable,

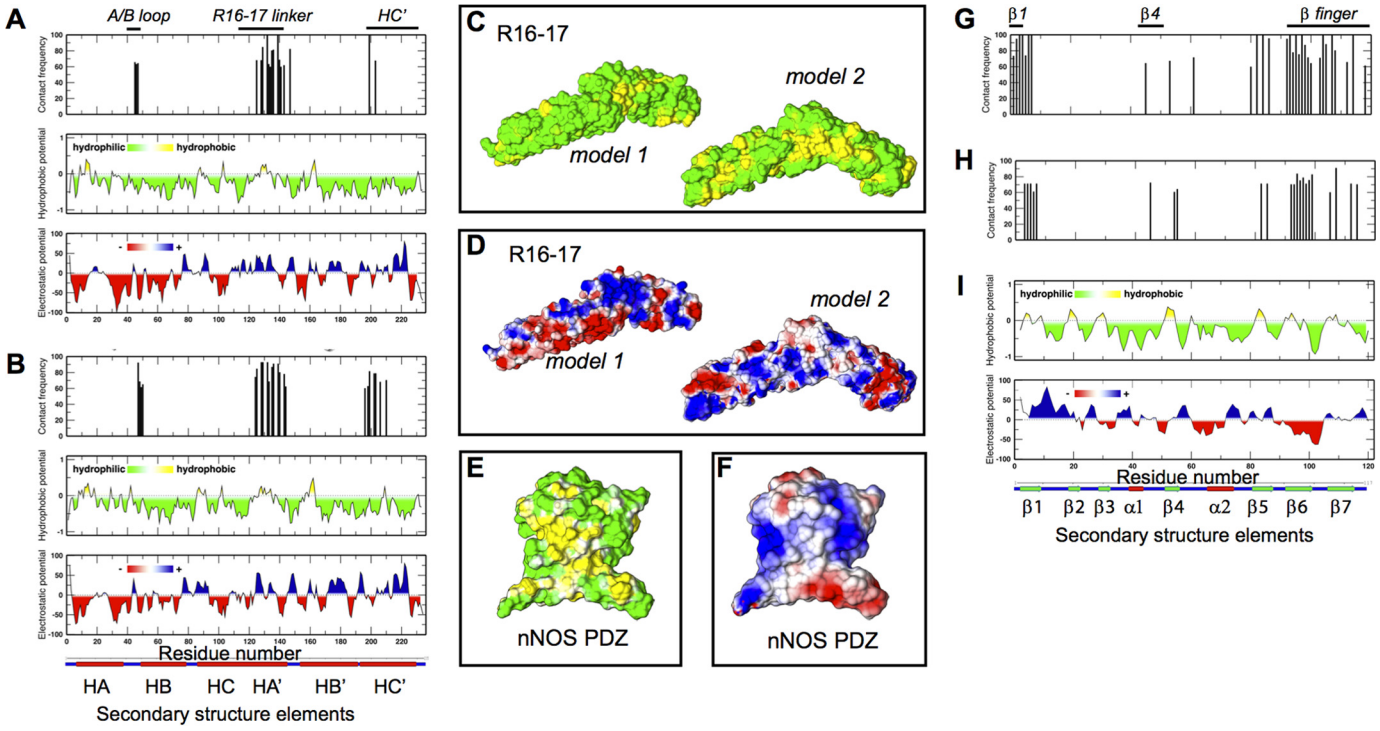

FIGURE 3. **Reciprocal contacts of the dystrophin R16–17 and the nNOS-PDZ domains on each other obtained by rigid docking.** Contact frequencies are obtained from the 20 best poses of rigid docking for the two SAXS-based models of dystrophin R16–17 and the homology model of the nNOS-PDZ domain. *A* and *B*, interaction sites with a high contact frequency (>60%) projected onto dystrophin R16–17 model 1 (*A*) and model 2 (*B*) are shown in *purple*. The contact frequency and profile of hydrophobic and electrostatic potentials are shown along the primary sequence of dystrophin R16–17 as a color gradient of *green to yellow* or *red to blue*, respectively. The secondary structure elements of dystrophin R16–17 are indicated at the *bottom* of *A* and *B* for clarity as follows: α-helices, *red*; loops, *blue*. *C* and *D*, surface potentials of the two dystrophin R16–17 models as obtained under SAXS volume restraints: platinum hydrophobicity (molecular hydrophobicity potential) is colored from *green* hydrophilic to *yellow* hydrophobic (*C*) and APBS electrostatics with *red* negative and *blue* positive for an isosurface of ±50 KT/e (K is Boltzmann constant) (*D*) with the same orientations as described in the legend to Fig. 2. *E* and *F*, surface potentials of the human nNOS-PDZ homology model are shown with similar representations as in *C* and *D*. *G-I*, contact frequency plots between the nNOS-PDZ domain and the two models 1 (*G*) and 2 (*H*) of dystrophin R16–17 are shown along the primary sequence of nNOS-PDZ. The hydrophobic and electrostatic potential profiles (*I*) of the nNOS-PDZ domain are shown. The secondary structural elements of the nNOS-PDZ domain are indicated at the bottom of (*I*) for clarity as follows: α-helices, *red*; loops, *blue*; and β-sheets, *green*.

we measured the melting temperature of the wild-type and mutated proteins using circular dichroism at 222 nm with increasing temperature from 15 to 85 °C. The melting temperatures varied from 59 to 75 °C, showing a high stability of the mutated proteins (Fig. 1*D*). The nNOS-PDZ protein had a typical β-strand-dominated CD spectrum with a molar ellipticity peak at 208 nm of ~8500 degrees cm^2 $dmol^{-1}$, as expected from its known structure, and a T_m of unfolding of 52 °C. Overall, these data allowed these proteins to be used to determine their dissociation constant with the nNOS-PDZ.

Binding Affinity of nNOS-PDZ for Syntrophin and Dystrophin R16–17—We first cloned, expressed, and produced the nNOS-PDZ partner and as a positive control, the PDZ domain of syntrophin (SNTA-PDZ), a known partner of nNOS-PDZ (Fig. 2*A*). The dissociation constant of dystrophin R16–17 toward nNOS-PDZ was determined using the BLItz technique to be 50 ± 6 μM. By contrast, the K_D for nNOS-PDZ to syntrophin was 7.2 ± 1.2 μM (Fig. 2*B*). This clear 5-fold weaker binding of nNOS-PDZ to dystrophin R16–17 than to syntrophin is consistent with the quantitative data previously obtained using the yeast two-hybrid system (18). There was no interaction of the two proteins with GST alone.

Alanine-scanning Mutagenesis Reveals Three Sites Involved in Dystrophin R16–17 Binding to nNOS-PDZ—The alanine mutants showed modifications of dissociation constants from 2-fold lower to 4-fold higher values compared with the wild-type value of 50 μM. A statistical comparison of the values showed that 15 of the 32 variants were significantly different, with 4 variants showing a decreased K_D and 11 showing a higher K_D compared with that of the wild-type (Fig. 2*C*). The mutated sites with significantly affected values can be categorized into three main regions (Fig. 2, *C-E*): a region in R16 near the A/B loop (*D–G* alanine mutation sites), a region involving part of the R16–17 linker (~10 residues) and the N-terminal end of R17 (*Q*, *R*, and *U* alanine mutation sites), and a region spanning most of helix C′ of R17 (*Z*, *AA*, *BB*, *CC*, *DD*, and *FF* alanine mutation sites). Some isolated residues also gave rise to a decrease or increase in the binding affinity, such as the *K* site on helix B of R16 and the *W* and *X* sites on helix B′ of R17. In addition, the Sb mutant similar to one previously shown to impair the nNOS-dystrophin interaction *in vivo* (18) showed a K_D of 130 ± 17 μM, which is three times weaker than the wild-type R16–17 construct.

In Silico Construction of a Dystrophin R16–17·nNOS-PDZ Complex

Three-dimensional Models of Both Partners—With the aim of designing a three-dimensional model of the dystrophin·nNOS complex, we built structural models of each protein. Two dystrophin R16–17 models (models 1 and 2) were obtained using

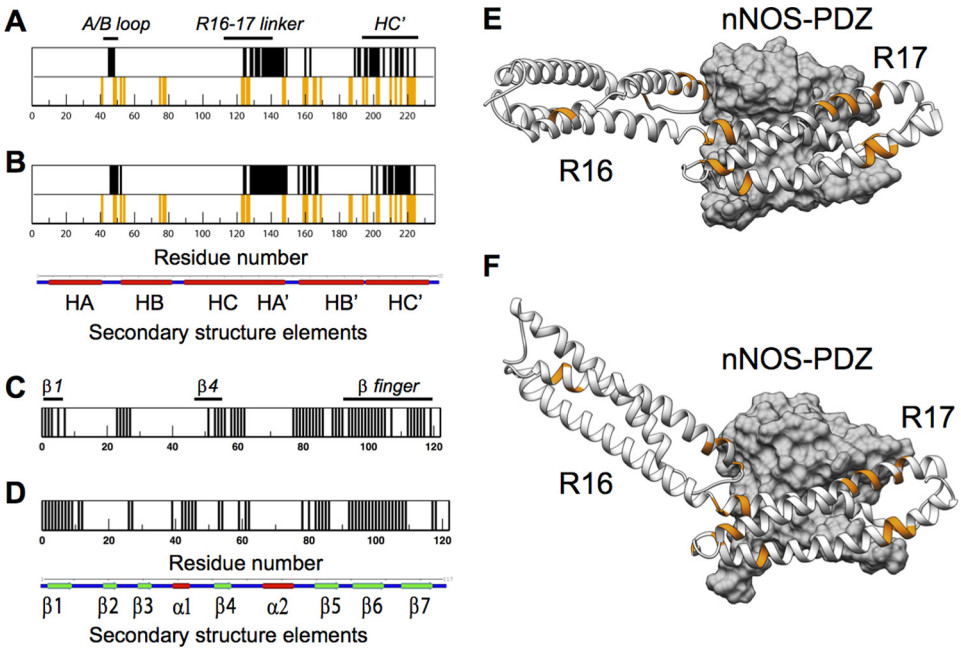

FIGURE 4. **Final dystrophin R16–17·nNOS-PDZ complexes obtained after interactive flexible docking.** *A* and *B*, contact mapping in the final complexes formed by the two SAXS-based models of dystrophin R16–17 with the homology model of the nNOS-PDZ domain are shown along dystrophin sequence. The structural elements of dystrophin R16–17 are shown *below* the diagram. The sites of alanine-scanning mutagenesis with significant differences in affinity are shown as *orange bars below* the contact maps of dystrophin R16–17. *C* and *D*, contact mapping in the final complexes formed by the two SAXS-based models of dystrophin R16–17 with the homology model of the nNOS-PDZ domain are shown along nNOS-PDZ sequence. *E* and *F*, flexible docking led to two three-dimensional nNOS-PDZ·dystrophin R16–17 structural complexes. The two dystrophin R16–17 models 1 (*E*) and 2 (*F*) are shown in the *gray schematic* and the nNOS-PDZ domain as a *gray volume*. The dystrophin residues inducing significantly different K_D for nNOS-PDZ binding are shown in *orange* as described in the legend to Fig. 2.

an approach combining small-angle x-ray scattering data and *in silico* reconstruction (24), and both showed that each repeat folded into a triple helical coiled-coil. The R16–17 linker presents different structural behavior in the two models (Fig. 2, *D* and *E*) because of a different relative orientation of the two successive repeats. Both models have been used to build the complex with nNOS, constituting a set of putative conformers for the dystrophin R16–17. Crystal structures of the nNOS-PDZ have been obtained from the rat isoform (15). Human and rat nNOS-PDZ sequences differed by 1 residue indeed the I-TASSER server (23) produced a human nNOS-PDZ homology model of high reliability (C-score of −0.03). The protein is composed of two α helices and seven β strands. The protein backbone of the human model is very similar to the experimental rat structures, with a backbone root mean square deviation of 0.8 Å toward the main structural pattern (Protein Data Bank code 1QAU).

Contact Surfaces Obtained by Low-resolution Rigid Docking—For a large exploration of the conformational space, rigid docking was performed at low-resolution using the two SAXS-based models of R16–17 and the homology model of human nNOS-PDZ. The contact frequencies were computed over the 20 best complexes with a cut-off distance of 5 Å to define the spatial proximity of two residues. The most frequent contact residues (>60%) on the two dystrophin R16–17 models indicated that three main regions are involved in the interaction with nNOS-PDZ (Fig. 3, *A* and *B*). These regions mainly correspond to (i) the A/B loop and N-terminal end of helix B of R16 involving residues Lys^{45} to Phe^{47} in model 1 (with the numbering of residues relative to the constructs presented in Fig. 2*A*) and Phe^{47} to Leu^{50} in model 2, (ii) the N-terminal end of R17 composed of residues Trp^{125} to Arg^{147} in model 1 and Lys^{124} to Gln^{144} in model 2, and (iii) helix C′ of R17 with residues Ile^{199} to Lys^{203} in model 1 and Asp^{196} to Arg^{210} in model 2. Whereas electrostatic properties of these three contact regions are balanced, they clearly constitute a large and homogenous three-dimensional hydrophobic patch (Fig. 3, *A–D*). Therefore, changes in charged residues for alanine may reinforce the hydrophobicity of several sites, thus inducing an increase in the binding affinity as observed for mutants D, F, K, and W. Reciprocally, the nNOS-PDZ regions involved in the binding with dystrophin are the (i) β1 region (residues 3 to 7), (ii) β4 region (residues 45 to 54), (iii) β5 region (residues 82–84), and (iv) β-finger region composed of β6 and β7 strands (residues 92–99 and 105–114) (Fig. 3, *G* and *H*)). The electrostatic profile of this contact interface shows contrasting potentials, however, it is mostly hydrophobic with the exception of the β-finger region (Fig. 3, *E–I*).

Refining the Contact Surface Using Flexible Docking—Interactive flexible docking was performed using the best poses previously obtained by rigid docking and allowed the improvement of the contact surface definition. In addition to the previously defined contact regions, a small region on the C-terminal end of helix B′ and the entire helix C′ of R17 seemed to be clearly involved in the dystrophin region binding to nNOS-PDZ (Fig. 4, *A* and *B*). The global contact surface increased from 1094 $Å^2$ to 1984 $Å^2$ for R16–17 model 1 and 1150 $Å^2$ to 1658 $Å^2$ for R16–17 model 2, contributing to a better stability of the complex. In addition, overlapping of the dystrophin R16–17 models with the regions highlighted by the alanine-scanning mutagen-

esis increased from 14 and 29% after rigid docking to 31 and 43% after flexible docking for R16–17 models 1 and 2, respectively. Similarly, the nNOS-PDZ region involving β4 and β5 is confirmed and the β-finger seemed definitively essential for the interaction (Fig. 4, *C* and *D*). The two final models of the complex are shown in Fig. 4, *E* and *F*.

In Silico Mutagenesis—To understand how alanine mutations could modify the binding affinity, we performed an *in silico* mutagenesis on the final models of the R16–17·nNOS-PDZ complex. The differential binding free energy (ΔΔ*G*) was calculated, showing that several mutation sites displayed significant changes after alanine mutation. ΔΔ*G* changes were mainly observed in three regions that largely overlapped with those previously indicated by the experimental alanine-scanning mutagenesis (Fig. 5*A*). We analyzed the surface property changes before and after *in silico* mutations for the two mutants at the F and G sites, which experimentally increased and decreased the binding affinity, respectively. The F mutation (sequence FEDLF into FAALF) locally increases the hydrophobic surface potential of dystrophin, which could explain the decrease in the K_D observed experimentally (Fig. 5*B*), considering the general hydrophobic nature of the R16–17/nNOS-PDZ interaction at this location. By contrast, the G mutation (sequence FKQE into FAQA) concerns only one residue (Lys^{52}) contributing to the interaction with nNOS-PDZ by forming a salt-bridge in the native complex, and this interaction is lost after mutation (Fig. 5*C*), which could explain the K_D increase that was observed experimentally. These results clearly indicate that the residues located in a continuous three-dimensional interface and involving the F, G, Q, R, and Z to DD and FF sites could be at the origin of the specificity of the dystrophin/nNOS interaction.

Comparison of the Native Dystrophin R16–17-nNOS Binding Site with Modifications Induced by In-frame Exon Deletions, as Observed in BMD Patients—The R16–17 binding site for nNOS-PDZ is coded by exons 42 to 46 of the *DMD* gene (38). This gene is therefore partly truncated in in-frame deletions of exons starting at exon 45 and involving two or more exons (2, 3). These deletions could or could not allow the reconstitution of a structure similar to a true repeat (39, 40). We determined the sequence similarities between the surface residues of the nNOS binding site of the native R17 (C-terminal part of helix B′ and helix C′) and the residues of the corresponding region in the reconstituted repeats after the deletion of exons 45–48, 45–51, 45–53, 45–55, and 45–57 (Fig. 6). These similarities were 20, 33, 27, 37, and 20%, respectively.

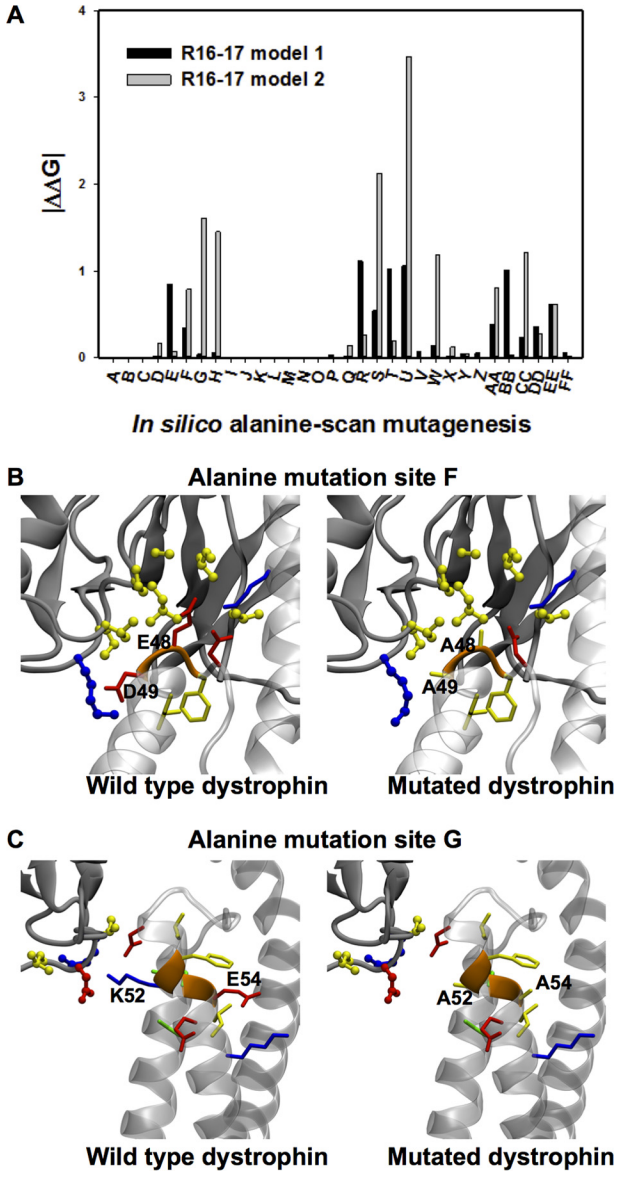

FIGURE 5. ***In silico* dystrophin R16–17 alanine-scanning mutagenesis and the effects of mutations on the interaction with the nNOS-PDZ domain.** *A*, average binding energy changes (ΔΔ*G*, in kcal mol^{-1}) as calculated by FoldX over the two models of R16–17·nNOS-PDZ complexes obtained through interactive flexible docking. Absolute values are provided to dampen the ΔΔ*G* modulations due to conformational changes observed between the two dystrophin R16–17 models. *B* and *C*, examples of R16–17 mutation sites producing either an increase or a decrease in the binding affinity for nNOS-PDZ. *B*, the F site induces an increase in the affinity of binding from K_D of 50 ± 6 for the wild-type to K_D of 20 ± 2 μM; *C*, the G site induces a decrease in the binding affinity to K_D of 125 ± 30 μM.

Discussion

In this study, we used two complementary approaches to construct structural models of the complex involving dystrophin repeats R16–17 and nNOS-PDZ. Alanine-scanning mutagenesis of charged residues using 32 variants of dystrophin R16–17 highlighted multiple regions where mutagenesis modified the binding affinity, indicating that these regions are involved in the interaction with nNOS. This experimental mapping combined with the rigid docking calculations showed that these essential regions can be reduced to a three-component binding interface, including (i) the A/B loop and extreme N-terminal part of helix B of R16, (ii) the C-terminal part of the linker between the two repeats (*i.e.* the N-terminal part of helix A′ of R17, primary binding site previously characterized *in vivo* (18)), and (iii) almost the entire helix C′ of repeat 17. This is in agreement with the binding affinity modulations observed for all the contact regions as noted by the alanine-scanning experiments. Therefore, our results clearly indicate that complex stability requires the involvement of not only the primary binding site in helix A′ of R17 but also the entire helix C′ of R17 and the extreme N-terminal part of helix B of R16.

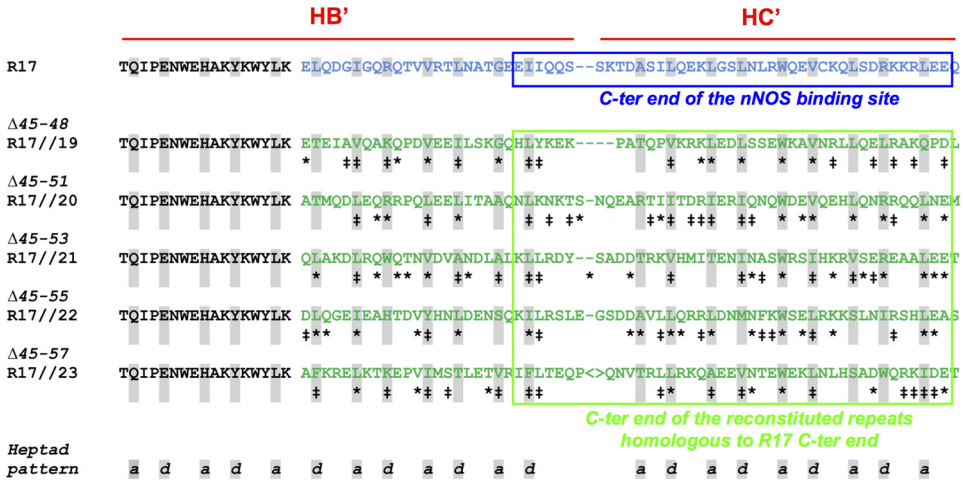

FIGURE 6. **Comparison of the native dystrophin R16–17/nNOS binding site with modifications induced by in-frame exon deletions as observed in BMD patients.** Five in-frame exon deletions as observed in BMD patients are shown: Δ45–48, Δ45–51, Δ45–53, Δ45–55, and Δ45–57. These deletions permit the reconstitution of a native-like repeat structure by concatenating the N-terminal part of R17 encoded by exon 44 (in *black*) and the C-terminal part of repeats R19, R20, R21, R22, and R23, denoted R17//19, R17//20, R17//21, R17//22 and R17//23 (in *green*), respectively. The residues encoded by exon 45 in the native R17 repeat are shown in *blue*. The *blue frame* highlights the nNOS-binding site region in wild-type R17, which is replaced after deletions by the corresponding sequences of the concatenated repeats (*green frame*). Sequence similarities (* for identity and ‡ for similarity) were compared for all residues except those involved in the heptad pattern (*a* and *d* positions highlighted in *gray*), which correspond to core residues not contributing to molecular surface properties.

The second flexible docking permitted the modulation of the binding interface by means of a modification of the R16–17 structure under fitting. This docking resulted in the additional involvement of two small regions of the helix B′ of R17 that overlap with the alanine-scanning mutants W and Z, which showed increased and decreased binding affinity toward nNOS, respectively. Finally, the regions involved in the interaction with nNOS are clearly the N-terminal end of helix B of R16 and helix A′, small spots of helix B′ and almost the entire helix C′ of R17. In contrast to previous hypotheses, R16 is only slightly involved, whereas R17 is profoundly involved in the interaction.

All these regions constitute a continuous tridimensional interaction platform. This platform is slightly modified in the two models of R16–17, indicating that the binding site could support small modulations in a dynamical context. Indeed, the remarkable correlation between the detailed structural analysis and the experimental alanine-scanning results strongly validates our structural models of the R16–17·nNOS-PDZ complex.

Our work also showed structural details of the nNOS-PDZ surface that are involved in binding to dystrophin. Despite the lack of a human crystallographic structure of the domain, high homology between the human and rat sequences allowed generation of a reliable structural model comprising the specific nNOS-PDZ β-finger composed of the two β-strands 6 and 7 (15). Interestingly, the contact frequency map of nNOS with dystrophin showed a consistent involvement in the interaction of this mainly negatively charged β-finger with the globally positive helix C of R17. The nNOS binding interface also involves the three β-strands 1, 4, and 5, which constitute a flat and hydrophobic front surface that strongly associates with the hydrophobic patch that we previously described at the dystrophin R16–17 surface (41). We noticed that similar interaction of a β-sheet with a coiled-coil structure has already been reported for the association of ZU5 domain of ankyrin to β-spectrin, involving A/B loop, A′ and C′ helices of the spectrin filament (42).

More interestingly, the nNOS front surface contacting dystrophin R16–17 is opposite to the platform that is classically involved in interaction with other PDZ domains, called glove, and formed by α1 helix and β2 and β3 strands. The comparison of the nNOS-PDZ interfaces that are involved in the binding with dystrophin R16–17 and with syntrophin-PDZ (15) showed a similar set of residues including Pro^{2} to Arg^{8}, Val^{83}, Ile^{85}, and His^{95} to Thr^{108}. To bind both syntrophin and dystrophin concurrently, a single nNOS homodimer should then involve either (i) its two PDZ domains present in a nNOS dimer, one PDZ with dystrophin and one PDZ with syntrophin, which could be achieved through the recently suggested great flexible position of the nNOS-PDZ domain toward the oxidase domain (14) or (ii) a binding interface of dystrophin R16–17 modified to accommodate the PDZ domains of both syntrophin and nNOS.

The R16 and R17 site of dystrophin involved in the binding to nNOS is strongly modified in the most common BMD in-frame deletions involving exon 45 and further exons (40). The deletion of exons 45 to 55 has been explored in detail regarding the presence or absence of the nNOS at the sarcolemma (11). This deletion deletes half of R17 at the C-terminal end, which is replaced by the equivalent part of R22, reconstituting the structure of a true repeat at the new junction (40) and maintaining the repeat phasing (43). Several patients who presented a nNOS at the sarcolemma were less diseased than patients whose nNOS was not present at the sarcolemma. These data were very striking, and the authors hypothesized that epigenetic factors or genetic modifiers may be involved in this regulation (11). We here questioned these data from another angle. As we know from the alanine-scanning mutagenesis that a single mutation of R16–17 can modify the affinity of the interaction, we could argue that non-synonymous mutations qualified as polymor-

phic in a native context could have a valuable effect in the deletion context on the affinity of the nNOS/dystrophin interaction. Some of these SNPs could restore an affinity of nNOS for the modified site of interaction. This restoration may be valuable for the two proteins, and SNPs of the two *DMD* and *NOS1* genes could have additive or subtractive effects. In a first approach, we compared the alignments of the sequences of several deletion mutants starting at exon 45, such as deletions 45–48, 45–51, 45–53, 45–55, and 45–57, which all reconstitute the structure of a native repeat at the new junction. The closest similarity in the nNOS binding site was determined for deletion 45–55 at 37% using the consensus sequence of the *DMD* gene. Therefore, it could be very valuable to obtain the gene sequence of BMD patients with the deletion 45–55 to determine whether the similarity to the native binding site is greater in the patients with a less severe phenotype.

Our study will help understand how the nNOS-dystrophin binding site is modified in in-frame deletions involving exon 42 coding for helix B of R16 to exon 46 coding for the C-terminal part of helix C of R17. It could be interesting in analyzing the results of therapy of DMD patients by exon skipping and in maintaining the true nNOS binding site in micro-dystrophins (4, 5, 19).

Author Contributions—O. D., J. F. H., N. M., and E. L. R. conceived the study and wrote most of the paper. A. E. M. and K. M. made most of the experiments, A. E. M. the *in silico* study and K. M. the biochemical study. All authors analyzed the results.

Acknowledgments—We acknowledge Sébastien Fiorucci and Martin Zacharias who provided the last version of the ATTRACT program. We also thank the synchrotron SOLEIL facility (St. Aubin) for allocating regular beam time and their dedicated staffs for technical help with the SWING beamline.

References

1. Koenig, M., Beggs, A. H., Moyer, M., Scherpf, S., Heindrich, K., Bettecken, T., Meng, G., Müller, C. R., Lindlöf, M., and Kaariainen, H. (1989) The molecular basis for Duchenne *versus* Becker muscular dystrophy: correlation of severity with type of deletion. *Am. J. Hum. Genet.* **45,** 498–506
2. Flanigan, K. M., Dunn, D. M., von Niederhausern, A., Soltanzadeh, P., Gappmaier, E., Howard, M. T., Sampson, J. B., Mendell, J. R., Wall, C., King, W. M., Pestronk, A., Florence, J. M., Connolly, A. M., Mathews, K. D., Stephan, C. M., Laubenthal, K. S., Wong, B. L., Morehart, P. J., Meyer, A., Finkel, R. S., Bonnemann, C. G., Medne, L., Day, J. W., Dalton, J. C., Margolis, M. K., Hinton, V. J., United Dystrophinopathy Project Consortium, and Weiss, R. B. (2009) Mutational spectrum of DMD mutations in dystrophinopathy patients: application of modern diagnostic techniques to a large cohort. *Hum. Mutat.* **30,** 1657–1666
3. Tuffery-Giraud, S., Béroud, C., Leturcq, F., Yaou, R. B., Hamroun, D., Michel-Calemard, L., Moizard, M. P., Bernard, R., Cossée, M., Boisseau, P., Blayau, M., Creveaux, I., Guiochon-Mantel, A., de Martinville, B., Philippe, C., Monnier, N., Bieth, E., Khau Van Kien, P., Desmet, F. O., Humbertclaude, V., Kaplan, J. C., Chelly, J., and Claustres, M. (2009) Genotype-phenotype analysis in 2,405 patients with a dystrophinopathy using the UMD-DMD database: a model of nationwide knowledgebase. *Hum. Mutat.* **30,** 934–945
4. Fairclough, R. J., Wood, M. J., and Davies, K. E. (2013) Therapy for Duchenne muscular dystrophy: renewed optimism from genetic approaches. *Nat. Rev. Genet.* **14,** 373–378
5. Wein, N., Alfano, L., and Flanigan, K. M. (2015) Genetics and emerging treatments for Duchenne and Becker muscular dystrophy. *Pediatr. Clin. N. Am.* **62,** 723–742
6. Le Rumeur, E., Winder, S. J., and Hubert, J. F. (2010) Dystrophin: more than just the sum of its parts. *Biochim. Biophys. Acta* **1804,** 1713–1722
7. Stamler, J. S., and Meissner, G. (2001) Physiology of nitric oxide in skeletal muscle. *Physiol. Rev.* **81,** 209–237
8. Sato, K., Yokota, T., Ichioka, S., Shibata, M., and Takeda, S. (2008) Vasodilation of intramuscular arterioles under shear stress in dystrophin-deficient skeletal muscle is impaired through decreased nNOS expression. *Acta Myol.* **27,** 30–36
9. Tengan, C. H., Rodrigues, G. S., and Godinho, R. O. (2012) Nitric oxide in skeletal muscle: role on mitochondrial biogenesis and function. *Int. J. Mol. Sci.* **13,** 17160–17184
10. Sander, M., Chavoshan, B., Harris, S. A., Iannaccone, S. T., Stull, J. T., Thomas, G. D., and Victor, R. G. (2000) Functional muscle ischemia in neuronal nitric oxide synthase-deficient skeletal muscle of children with Duchenne muscular dystrophy. *Proc. Natl. Acad. Sci. U.S.A.* **97,** 13818–13823
11. Gentil, C., Leturcq, F., Ben Yaou, R., Kaplan, J. C., Laforet, P., Pénisson-Besnier, I., Espil-Taris, C., Voit, T., Garcia, L., and Piétri-Rouxel, F. (2012) Variable phenotype of del45–55 Becker patients correlated with nNOSmu mislocalization and RYR1 hypernitrosylation. *Hum. Mol. Genet.* **21,** 3449–3460
12. Wang, Y., Newton, D. C., and Marsden, P. A. (1999) Neuronal NOS: gene structure, mRNA diversity, and functional relevance. *Crit. Rev. Neurobiol.* **13,** 21–43
13. Förstermann, U., and Sessa, W. C. (2012) Nitric oxide synthases: regulation and function. *Eur. Heart J.* **33,** 829–837
14. Campbell, M. G., Smith, B. C., Potter, C. S., Carragher, B., and Marletta, M. A. (2014) Molecular architecture of mammalian nitric oxide synthases. *Proc. Natl. Acad. Sci. U.S.A.* **111,** E3614–3623
15. Hillier, B. J., Christopherson, K. S., Prehoda, K. E., Bredt, D. S., and Lim, W. A. (1999) Unexpected modes of PDZ domain scaffolding revealed by structure of nNOS-syntrophin complex. *Science* **284,** 812–815
16. Zhou, L., and Zhu, D. Y. (2009) Neuronal nitric oxide synthase: structure, subcellular localization, regulation, and clinical implications. *Nitric Oxide* **20,** 223–230
17. Lai, Y., Thomas, G. D., Yue, Y., Yang, H. T., Li, D., Long, C., Judge, L., Bostick, B., Chamberlain, J. S., Terjung, R. L., and Duan, D. (2009) Dystrophins carrying spectrin-like repeats 16 and 17 anchor nNOS to the sarcolemma and enhance exercise performance in a mouse model of muscular dystrophy. *J. Clin. Invest.* **119,** 624–635
18. Lai, Y., Zhao, J., Yue, Y., and Duan, D. (2013) alpha2 and alpha3 helices of dystrophin R16 and R17 frame a microdomain in the alpha1 helix of dystrophin R17 for neuronal NOS binding. *Proc. Natl. Acad. Sci. U.S.A.* **110,** 525–530
19. Harper, S. Q. (2013) Molecular dissection of dystrophin identifies the docking site for nNOS. *Proc. Natl. Acad. Sci. U.S.A.* **110,** 387–388
20. Tochio, H., Zhang, Q., Mandal, P., Li, M., and Zhang, M. (1999) Solution structure of the extended neuronal nitric oxide synthase PDZ domain complexed with an associated peptide. *Nat. Struct. Biol.* **6,** 417–421
21. Mirza, A., Sagathevan, M., Sahni, N., Choi, L., and Menhart, N. (2010) A biophysical map of the dystrophin rod. *Biochim. Biophys. Acta* **1804,** 1796–1809
22. Gibson, D. G. (2011) Enzymatic assembly of overlapping DNA fragments. *Methods Enzymol.* **498,** 349–361
23. Zhang, Y. (2009) I-TASSER: fully automated protein structure prediction in CASP8. *Proteins* **77,** 100–113
24. Molza, A.-E., Férey, N., Czjzek, M., Le Rumeur, E., Hubert, J.-F., Tek, A., Laurent, B., Baaden, M., and Delalande, O. (2014) Innovative Interactive Flexible Docking method for multi-scale reconstruction elucidates dystrophin molecular assembly. *Faraday Discuss.* **169,** 45–62
25. Pérez, J., and Nishino, Y. (2012) Advances in X-ray scattering: from solution SAXS to achievements with coherent beams. *Curr. Opin. Struct. Biol.* **22,** 670–678
26. Petoukhov, M. V., and Svergun, D. I. (2007) Analysis of X-ray and neutron scattering from biomacromolecular solutions. *Curr. Opin. Struct. Biol.* **17,** 562–571
27. Petoukhov, M. V., Franke, D., Shkumatov, A. V., Tria, G., Kikhney, A. G.,

Gajda, M., Gorba, C., Mertens, H. D., Konarev, P. V., and Svergun, D. I. (2012) New developments in the ATSAS program package for small-angle scattering data analysis. *J. Appl. Crystallogr.* **45,** 342–350
28. Schneider, S., Saladin, A., Fiorucci, S., Prévost, C., and Zacharias, M. (2012) ATTRACT and PTools: open source programs for protein-protein docking. *Methods Mol. Biol.* **819,** 221–232
29. Tek, A., Chavent, M., Baaden, M., Delalande, O., Bourdot, P., and Férey, N. (eds) (2012) Advances in human-protein interaction: interactive and immersive molecular simulations. In *Protein-Protein Interactions: Computational and Experimental Tools* (Cai, W., and Hong, H., eds), pp. 27–64, InTech, Rijeka, Croatia
30. Baker, N. A., Sept, D., Joseph, S., Holst, M. J., and McCammon, J. A. (2001) Electrostatics of nanosystems: application to microtubules and the ribosome. *Proc. Natl. Acad. Sci. U.S.A.* **98,** 10037–10041
31. Krieger, E., Darden, T., Nabuurs, S. B., Finkelstein, A., and Vriend, G. (2004) Making optimal use of empirical energy functions: force-field parameterization in crystal space. *Proteins* **57,** 678–683
32. Kabsch, W., and Sander, C. (1983) Dictionary of protein secondary structure: pattern recognition of hydrogen-bonded and geometrical features. *Biopolymers* **22,** 2577–2637
33. Pyrkov, T. V., Chugunov, A. O., Krylov, N. A., Nolde, D. E., and Efremov, R. G. (2009) PLATINUM: a web tool for analysis of hydrophobic/hydrophilic organization of biomolecular complexes. *Bioinformatics* **25,** 1201–1202
34. Dolinsky, T. J., Czodrowski, P., Li, H., Nielsen, J. E., Jensen, J. H., Klebe, G., and Baker, N. A. (2007) PDB2PQR: expanding and upgrading automated preparation of biomolecular structures for molecular simulations. *Nucleic Acids Res.* **35,** W522–525
35. Pettersen, E. F., Goddard, T. D., Huang, C. C., Couch, G. S., Greenblatt, D. M., Meng, E. C., and Ferrin, T. E. (2004) UCSF Chimera: a visualization system for exploratory research and analysis. *J. Comput. Chem.* **25,** 1605–1612
36. Humphrey, W., Dalke, A., and Schulten, K. (1996) VMD-visual molecular dynamics. *J. Mol. Graph.* **14,** 33–38
37. Van Durme, J., Delgado, J., Stricher, F., Serrano, L., Schymkowitz, J., and Rousseau, F. (2011) A graphical interface for the FoldX forcefield. *Bioinformatics* **27,** 1711–1712
38. Koenig, M., and Kunkel, L. M. (1990) Detailed analysis of the repeat domain of dystrophin reveals four potential hinge segments that may confer flexibility. *J. Biol. Chem.* **265,** 4560–4566
39. Nicolas, A., Lucchetti-Miganeh, C., Yaou, R. B., Kaplan, J. C., Chelly, J., Leturcq, F., Barloy-Hubler, F., and Le Rumeur, E. (2012) Assessment of the structural and functional impact of in-frame mutations of the *DMD* gene, using the tools included in the eDystrophin online database. *Orphanet. J. Rare Dis.* **7,** 45
40. Nicolas, A., Raguénès-Nicol, C., Ben Yaou, R., Ameziane-Le Hir, S., Chéron, A., Vié, V., Claustres, M., Leturcq, F., Delalande, O., Hubert, J. F., Tuffery-Giraud, S., Giudice, E., Le Rumeur, E., French Network of Clinical Reference Centres for Neuromuscular Diseases (CORNEMUS) (2015) Becker muscular dystrophy severity is linked to the structure of dystrophin. *Hum. Mol. Genet.* **24,** 1267–1279
41. Giudice, E., Molza, A.-E., Laurin, Y., Nicolas, A., Le Rumeur, E., and Delalande, O. (2013) Molecular clues to the dystrophin: nNOS interaction: a theoretical approach. *Biochemistry* **52,** 7777–7784
42. Ipsaro, J. J., Harper, S. L., Messick, T. E., Marmorstein, R., Mondragón, A., and Speicher, D. W. (2010) Crystal structure and functional interpretation of the erythrocyte spectrin tetramerization domain complex. *Blood* **115,** 4843–4852
43. Harper, S. Q., Hauser, M. A., DelloRusso, C., Duan, D., Crawford, R. W., Phelps, S. F., Harper, H. A., Robinson, A. S., Engelhardt, J. F., Brooks, S. V., and Chamberlain, J. S. (2002) Modular flexibility of dystrophin: implications for gene therapy of Duchenne muscular dystrophy. *Nat. Med.* **8,** 253–261